

Si AND Mn ABUNDANCES IN DAMPED LYMAN α SYSTEMS WITH LOW DUST CONTENT¹

MAX PETTINI AND SARA L. ELLISON

Institute of Astronomy, Madingley Road, Cambridge, CB3 0HA, UK

CHARLES C. STEIDEL² AND ALICE E. SHAPLEY

Palomar Observatory, Caltech 105-24, Pasadena, CA 91125

DAVID V. BOWEN

Princeton University Observatory, Princeton, NJ 08544

¹The data presented herein were obtained with the NASA/ESA *Hubble Space Telescope* and with the Keck I Telescope. The W.M. Keck Observatory is operated as a scientific partnership among the California Institute of Technology, the University of California, and the National Aeronautics and Space Administration. The Observatory was made possible by the generous financial support of the W.M. Keck Foundation.

²NSF Young Investigator

ABSTRACT

We have measured the abundances of Zn, Si, Mn, Cr, Fe, and Ni in three damped Lyman α systems at redshifts $z_{\text{abs}} \leq 1$ from high resolution echelle spectra of QSOs recorded with the Keck I telescope. In all three cases the abundances of Cr, Fe, and Ni relative to Zn indicate low levels of dust depletions. We propose that when the proportion of refractory elements locked up in dust grains is less than about 50%, it is plausible to assume an approximately uniform level of depletion for all grain constituents and, by applying a small dust correction, recover the intrinsic abundances of Si and Mn. We use this approach on a small sample of damped systems (6 – 8 cases) for which it is appropriate, with the aim of comparing the metallicity dependence of the ratios [Si/Fe] and [Mn/Fe] with analogous measurements in Milky Way stars. The main conclusion is that the relative abundances of both elements in distant galaxies are broadly in line with expectations based on Galactic data. Si displays a mild enhancement at low metallicities, as expected for an α -capture element, but there are also examples of near-solar [Si/Fe] at [Fe/H] < -1 . The underabundance of Mn at low metallicities is possibly even more pronounced than that in metal-poor stars, and no absorption system has yet been found where [Mn/Fe] is solar. The heterogeneous chemical properties of damped Lyman α systems, evident even from this limited set of measurements, provide further support for the conclusion from imaging studies that a varied population of galaxies gives rise to this class of QSO absorbers.

We also present a *Hubble Space Telescope* image of the field of one of the QSOs, Q0058+019, showing the presence of an edge-on late-type galaxy only 1.2 arcseconds from the absorption sight-line. If this is the galaxy producing the damped Lyman α system at $z_{\text{abs}} = 0.61251$, it is of relatively low luminosity ($M_B = -19.1$) and at an impact parameter of $10 h_{50}^{-1}$ kpc.

Subject headings: cosmology:observations — galaxies:abundances — galaxies:evolution — quasars:absorption lines

1. INTRODUCTION

This is the fourth paper in a series dealing with metal abundances in damped Lyman α systems (DLAs) at intermediate redshifts ($z_{\text{abs}} < 1.5$). The number of such systems known has been increasing slowly over the past few years with the growing database of *Hubble Space Telescope* (HST) QSOs observed at wavelengths below 3000 Å which are inaccessible from the ground. In Pettini et al. (1999, Paper III) we combined measurements of the abundance of Zn in 10 DLAs at $z_{\text{abs}} < 1.5$ with earlier surveys at higher redshifts to determine the evolution of the metallicity of H I gas in the universe. We found that, somewhat surprisingly, the metal content of DLAs apparently does not increase with cosmic time, and that the column density-weighted mean value of the Zn abundance remains roughly constant at $[\langle \text{Zn}/\text{H} \rangle] \simeq -1.1 \pm 0.2$ between $z = 3$ and 0.4.³ This result is apparently at odds with the common interpretation of DLAs as the high redshift progenitors of present day spiral galaxies; disk stars in the Milky Way, for example, had already reached $[\text{Fe}/\text{H}] \approx -0.5$ at $z \approx 1$ (Edvardsson et al. 1993), a point first made by Meyer & York (1992). The persisting low metallicity of DLAs may be explained by abundance gradients (Prantzos & Silk 1998) but, more generally, is consistent with the finding from *HST* imaging that galaxies of different morphological types and with a range of surface brightnesses contribute to the absorption cross-section for H I (Le Brun et al. 1997). To some extent this may well be a consequence of the fact that DLAs selected with *HST* are likely to be preferentially dust- and therefore metal-poor, simply because the background QSOs would otherwise be too faint to be accessible with a 2.5 m telescope.

Whatever the connection between them and present-day galaxies, damped Lyman α systems remain our best route to accurate determinations of element abundances at high redshifts. Element ratios in Galactic stars and nearby H II regions have long been scrutinized with a view to deciphering the clues they hold both to the origin of different stellar populations and to the stellar yields (see, for example, Wheeler, Sneden, & Truran 1989 for a review of the main ideas underlying this field of work). As pointed out by Pettini, Lipman, & Hunstead (1995), abundance measurements in DLAs are potentially an important extension of this technique (and one yet to be fully exploited), allowing access to elements which are not well observed in stars, to lower metallicities than those of present-day H II regions, and to a wider range of environments and physical conditions than local studies. A possible complication in interpreting interstellar abundances is accounting for the fractions of refractory elements which are missing from the gas-phase having been incorporated into dust grains; however, we are aided in this respect by the generally low dust depletions which seem to apply to many DLAs (Pettini et al. 1997a).

In this paper we analyse Keck I HIRES observations of several elements, ranging from Mg to Zn, in three DLAs at $z_{\text{abs}} \lesssim 1$. One of these, at $z_{\text{abs}} = 0.61251$ in Q0058+019 (= PHL 938), has not been studied before while for the other two, at $z_{\text{abs}} = 1.00945$ in Q0302–223 and $z_{\text{abs}} =$

³In the usual notation, $[\text{Zn}/\text{H}] = \log (\text{Zn}/\text{H}) - \log (\text{Zn}/\text{H})_{\odot}$.

0.85967 in Q0454+039, we previously published only intermediate resolution observations (Pettini & Bowen 1997, Paper II; Steidel et al. 1995, Paper I respectively). In addition, we present an *HST* WFPC2 image of the field of Q0058+019 where we resolve a galaxy which is a highly plausible candidate for the damped absorber, being very close to the QSO sight-line. We use the pattern of element abundances in these and other DLAs where corrections for dust depletion are estimated to be small to explore the metallicity dependence of the abundances of Si (an α -element) and Mn.

2. *HST* OBSERVATIONS

2.1. FOS Spectroscopy

A trawl of the *HST* Faint Object Spectrograph (FOS) data archive revealed that Q0058+019 exhibits a damped Lyman α line at $\lambda_{\text{obs}} = 1959 \text{ \AA}$, shown in Figure 1. In producing this spectrum we resampled the pipeline calibrated data to a linear dispersion of 0.51 \AA per pixel (one quarter diode steps) and applied a correction of +8% of the continuum level to bring the core of the Lyman α line to net zero flux. A fit to the absorption profile yielded a neutral hydrogen column density $N(\text{H}^0) = (1.2 \pm 0.5) \times 10^{20} \text{ cm}^{-2}$ at an absorption redshift $z_{\text{abs}} = 0.6118$. The column density error, which includes the effect of the correction applied to the zero level, is larger than is usually the case because the signal-to-noise ratio of the short FOS exposure is only ≈ 7 . Even so, the value of $N(\text{H}^0)$ is lower than the threshold $N(\text{H}^0) = 2 \times 10^{20} \text{ cm}^{-2}$ for DLAs originally adopted by Wolfe et al. (1986), reflecting the shift of the column density distribution toward lower values at $z < 1.5$, as first noted by Lanzetta, Wolfe, & Turnshek (1995). The difference between the redshift of the Lyman α line and $z_{\text{abs}} = 0.61251$ measured from the metal absorption lines in the HIRES spectrum (§3) corresponds to approximately half a diode on the detector and is typical of the accuracy with which the zero point of the FOS wavelength scale can be determined (Rosa, Kerber, & Keyes 1998).

The FOS spectra of Q0302–223 and Q0454+039 have been described in Papers II and I respectively; from a re-examination of the damped Lyman α line profiles we deduce $N(\text{H}^0) = (2.3 \pm 0.5) \times 10^{20} \text{ cm}^{-2}$ and $(4.9 \pm 0.7) \times 10^{20} \text{ cm}^{-2}$ at $z_{\text{abs}} = 1.00945$ and $z_{\text{abs}} = 0.85967$ respectively, in good agreement with the values published in the earlier papers.

2.2. WFPC2 Imaging

The field of Q0058+019 was imaged with the Wide Field Planetary Camera (WFPC2) as part of a larger *HST* program to study the morphology and environments of galaxies producing Mg II absorption systems. A set of four exposures was taken through the F702W filter (with an effective wavelength of 6900 \AA) in a two-point dither pattern; the total exposure time was 5000 s. The individual CCD frames were reduced using the pipeline calibration procedure and then coadded

by “drizzling” onto a master output pixel grid using the DITHER and DITHERII IRAF packages (Fruchter & Hook 1999).

The next step involved subtracting the QSO image to reveal any galaxies at small separations. The *HST* Mg II absorber imaging program was purposefully designed to facilitate this subtraction process by constructing an empirical point spread function (PSF) using images of many QSOs. Since the PSF characteristics (FWHM, shape, bleeding) depend sensitively on the level of saturation, QSOs observed in the program were grouped by flux so that an appropriate PSF could be determined using only QSOs of similar flux to Q0058+019. Subtraction of this median PSF (with the DAOPHOT IRAF package) then yielded the final image reproduced in Figure 2.

A faint galaxy is clearly visible approximately 1.2 arcsec to the north-east of the QSO. Given its proximity to the QSO sight-line this is the most likely candidate for the damped Lyman α absorber at $z_{\text{abs}} = 0.61251$. Apparently the model PSF does not reproduce accurately one of the diffraction spikes in the QSO image, leaving a residual flux deficit which cuts through the galaxy. When this is taken into account, the object morphology is suggestive of a late-type galaxy seen at a high inclination angle, $i \approx 65^\circ$. Table 1 lists relevant measurements, assuming $z_{\text{gal}} = 0.61251$ and adopting a $H_0 = 50 \text{ km s}^{-1} \text{ Mpc}^{-1}$, $q_0 = 0.05$ cosmology. We converted the measured F702W magnitude to an AB magnitude in the \mathcal{R} photometric system of Steidel & Hamilton (1993) by reference to ground-based images of the field (the [6930/1500] \mathcal{R} filter is a very close match to the WFPC2 F702W filter), and obtained $\mathcal{R} = 23.7$. For the above cosmology this in turn corresponds to an absolute magnitude in the rest-frame B -band (in the conventional Vega-based magnitude system) $M_B = -19.1$. No K-correction was applied because at $z = 0.61251$ 6930 Å is close to the effective wavelength of the B -band. Adopting $M_B^* = -21.0$ (e.g. Folkes et al. 1999), we conclude that the candidate damped Lyman α absorber is a galaxy of relatively low luminosity, with $L \simeq 1/6L^*$. Other DLAs have been found to be associated with compact galaxies, dwarfs, low surface brightness galaxies, and even an S0 (Le Brun et al. 1997; Lanzetta et al. 1997; Rao & Turnshek 1998). We now add a low luminosity spiral to the list and thereby reinforce the conclusion of these earlier studies that damped Lyman α systems are drawn from a diverse population of galaxies with a wide range of morphologies and luminosities.

3. KECK OBSERVATIONS

The spectra of the three QSOs were recorded at high spectral resolution with the HIRES echelle spectrograph (Vogt et al. 1994) on the Keck I telescope on Mauna Kea, Hawaii on 23 and 24 September 1998. Relevant details of the observations are collected in Table 2. We used the UV-blazed cross-disperser grating to record interstellar lines of interest in the three DLAs longward of the atmospheric cut-off near 3200 Å. Thus, in Q0058+019 we cover from Zn II $\lambda 2026$ to Mg I $\lambda 2852$ at $z_{\text{abs}} = 0.61251$, while the spectra of Q0302–223 and Q0454+039 extend from Si II $\lambda 1808$ to Mn II $\lambda 2606$ at $z_{\text{abs}} = 1.00945$ and 0.85967 respectively (for Q0302–223 this

necessitated a second grating setting). Given the good seeing (0.5 to 0.7 arcsec), we used the 0.86 arcsec wide entrance slit which projects to 3 pixels on the 2048x2048 Tektronix CCD detector resulting in a resolution of 6.5 km s^{-1} FWHM.

The echelle spectra were extracted with Tom Barlow’s customised software package, following the steps described in Paper III. The signal-to-noise ratios of the reduced spectra were measured directly from the rms fluctuations about the continuum level. In general the value of S/N varies along each spectrum due to the presence of broad emission lines at the QSO redshifts and increasing atmospheric absorption below 3600 \AA ; the values (per pixel) listed in column (10) of Table 2 refer to the region near rest frame wavelength $\lambda_0 = 2350 \text{ \AA}$ and should be representative of most of the absorption lines recorded. As can be seen from column (11) our Keck spectra are sensitive to rest frame equivalent widths of only a few m \AA . Figures 3, 4, and 5 show examples of absorption lines of varying strengths in each damped system.

4. ION COLUMN DENSITIES AND ELEMENT ABUNDANCES

When recorded at high spectral resolution the metal lines in QSO absorption systems commonly break up into multiple components; as can be seen from Figures 3, 4, and 5, the three DLAs observed here are no exception with the strongest absorption lines extending over 100 to 200 km s^{-1} . We analysed these complex absorption profiles with the VPFIT software written by Bob Carswell. The procedure has been described in detail before (e.g Paper III). As our data include seven transitions of Fe II with widely different f -values, spanning a range of ~ 165 , the model fits produced with VPFIT are well constrained and allow us to determine the redshift, velocity dispersion parameter b ($b = \sqrt{2}\sigma$, where σ is the one-dimensional velocity dispersion of the ions along the line of sight, assumed to be Gaussian), and ion column density N of each component. Details of the profile fits are collected in Table 3. The important point is that the total ion column densities do not depend on the fine detail of the profile decomposition because for each species considered we observe sufficiently weak transitions that the corresponding absorption lines fall on the linear part of the curve of growth. The exception is the Mg II $\lambda\lambda 2796, 2803$ doublet which is strongly saturated (see Figure 3) and is therefore not included in the present analysis.

The total column densities of the first ions of Zn, Si, Mn, Cr, Fe, and Ni in each DLA are listed in Table 4, together with $N(\text{H}^0)$. In deriving these values we used the compilation of f -values by Morton (1991) with the revisions proposed by Savage & Sembach (1996). For Ni II we took advantage of the recent radiative lifetime measurements by Fedchack & Lawler (1999) which have led to a reduction by a factor of 1.9 of the f -values of the $\lambda 1709.600$ and $\lambda 1741.549$ transitions relative to the values proposed by Zsargó & Federman (1998). The ensuing upward revision of $N(\text{Ni}^+)$ by a factor of $\simeq 2$ is significant for the interpretation of the pattern of relative element abundances, as discussed below (§5).

Since in DLAs the elements considered here are predominantly singly ionized, their abundances can be deduced directly by dividing the values of N in columns (4) to (9) by the values of $N(\text{H}^0)$ in column (3) of Table 4. Comparison with the solar system abundance scale of Anders & Grevesse (1989) finally gives the relative abundances listed in Table 5. (We have included in Table 5 the abundance measurements from Paper III, with the appropriate revisions for $N(\text{Ni}^+)$, as they will be considered in the discussion below.) We now briefly describe the results for the three DLAs which are the subject of the present paper.

1. Q0058+019; $z_{\text{abs}} = 0.61251$: Among the species observed in our HIRES spectra Zn gives the most direct measure of metallicity, free from the complication of dust depletion. In this low redshift DLA the Zn II $\lambda 2026, 2062$ doublet lines fall at 3267 and 3326 Å respectively, where observations are difficult due to atmospheric absorption. Although noisy, we clearly detect both lines; given the relatively low column density of hydrogen in this system, the presence of Zn II absorption in itself implies high abundances and indeed we deduce $[\text{Zn}/\text{H}] \approx 0$. The conclusion that this absorber has near-solar metallicity does not rest on the poorly observed Zn II lines alone; as can be seen from Table 5, the abundances of Cr and Fe, two other iron-peak elements, are also within a factor of ~ 2 of solar and could be higher if some fraction of these elements has been incorporated into dust grains, as discussed below (§5).

Evidently, DLAs with near-solar abundances are not rare at $z \lesssim 1$; out of the six measurements available to date, three have metallicities $Z_{\text{DLA}} \gtrsim 1/3Z_{\odot}$ (see Figure 7 of Paper III). However, a wide range of values of $[\text{Zn}/\text{H}]$, spanning ~ 1.5 dex, persists at all redshifts. It is intriguing that systems with high metallicity are invariably at the low end of the distribution of neutral hydrogen column density, so that the census of metals seen in absorption is dominated by gas with high $N(\text{H}^0)$ and low metal content.⁴ It is highly likely that selection effects play a role here; DLAs with large columns of molecules (and therefore probably high metallicity) are known to exist (e.g. the $z_{\text{abs}} = 0.68466$ 21 cm absorber towards B0218+357—Carilli, Rupen, & Yanny 1993; Wiklind & Combes 1995), but are too faint to be studied spectroscopically at optical and ultraviolet wavelengths. It is a lingering concern, however, that such selection effects are still largely unquantified.

Galaxies in the local universe exhibit a rough correlation between metallicity and B -band luminosity which apparently persists at least to $z = 0.4$ (Kobulnicky & Zaritsky 1999). Referring to these authors' Figure 4 it can be seen that, with $M_B = -19.1$ and $[\text{Zn}/\text{H}] = +0.1 \pm 0.2$, the $z_{\text{abs}} = 0.61251$ absorbing galaxy in Q0058+019 is somewhat metal-rich for its luminosity but is not inconsistent with the local relationship given the observed scatter. What is perhaps more remarkable is to find a near-solar abundance at relatively large distances from the centre of the galaxy. If the DLA arises in the disk, the high inclination of the galaxy, $i \approx 65^\circ$, places it at a galactocentric distance of $10 h_{50}^{-1}/\cos i \simeq 24 h_{50}^{-1}$ kpc. If the absorption takes place in the halo, it

⁴Thus, the new measurement for this DLA has a minimal effect on the column-density weighted average $[\langle \text{Zn}/\text{H} \rangle] = -1.03 \pm 0.23$ in the redshift interval $z = 0.40 - 1.5$ derived in Paper III.

would imply the existence of a cloud with $N(\text{H I}) = 10^{20} \text{ cm}^{-2}$ and solar metallicity $10 h_{50}^{-1} \text{ kpc}$ above the mid-plane of the galaxy. In either case it would seem that this galaxy does not have a marked abundance gradient, either along or perpendicular to the disk.

2. Q0302–223; $z_{\text{abs}} = 1.00945$: As can be seen from Figure 4, two main groups of components, separated by 36 km s^{-1} , produce most of the absorption seen in this DLA; additional weaker components, at $v = +35$ and $+121 \text{ km s}^{-1}$ relative to $z_{\text{abs}} = 1.00945$ are visible in the stronger Fe II lines. Although the Zn II and Cr II lines are weak, the corresponding column densities and abundances in Tables 3 and 4 are in excellent agreement with the values reported in Paper II which were measured from data of much lower resolution (0.88 \AA compared to 0.08 \AA FWHM). *HST* WFPC2 imaging (Le Brun et al. 1997) has revealed two compact galaxies close to the line of sight. At $z = 1.009$ they would have absolute luminosities $L_B \approx 0.2L_B^*$ and $\approx L_B^*$ and impact parameters $12 h_{50}^{-1}$ and $27 h_{50}^{-1} \text{ kpc}$ respectively. It remains to be established with spectroscopic observations which of the two galaxies is associated with the damped absorber.

3. Q0454+039; $z_{\text{abs}} = 0.85967$: Two groups of components, separated by 70 km s^{-1} , are responsible for most of the absorption in this DLA (Figure 5). Again, the column densities we deduce for Zn^+ , Cr^+ , and Fe^+ are in excellent agreement with the values measured by Steidel et al. (1995) from 2.3 \AA resolution Lick spectra, once allowance is made for the different f -values used. These authors also reported the presence of a compact galaxy close to the line of sight to the QSO, subsequently confirmed with WFPC2 images by Le Brun et al. (1997). If this is the absorber, it is at a projected separation of $8h_{50}^{-1} \text{ kpc}$ and it has an absolute luminosity $L_B \approx 0.25L_B^*$. The low element abundances we find, approximately 1/10 of solar, indicate that this galaxy apparently does not conform to the metallicity-luminosity relation discussed by Kobulnicky & Zaritsky (1999); in this respect it is more in line with present-day H II galaxies.

5. DUST DEPLETIONS

The pattern of relative abundances measured in the interstellar gas of distant galaxies responds to two effects, the selective depletion of refractory elements onto dust grains and inherent differences from the solar system scale, reflecting the past history of star formation which may well have been different from that of the Milky Way disk. Our goal here is to separate these two effects and, by accounting for the first, gain an insight into the second. In this endeavour we are guided by the extensive body of data on element abundances in stellar populations and the interstellar medium (ISM) of our Galaxy.

Of the elements considered here, Zn, Cr, Fe, and Ni all track each other closely in Galactic stars with metallicities $-2.0 \leq [\text{Fe}/\text{H}] \leq 0.0$ (e.g. Ryan, Norris, & Beers 1996). Dust depletion, on the other hand, is more significant for Cr, Fe, and Ni than for the generally undepleted Zn (Savage & Sembach 1996). It follows from these considerations that we can take the ratios $[\text{Zn}/\text{Cr}]$,

[Zn/Fe], and [Zn/Ni] as indicative of the fractions of these refractory elements which are missing from the gas-phase, e.g.

$$[\text{Zn/Cr}] = \log \left(\frac{f_{\text{gas}} + f_{\text{dust}}}{f_{\text{gas}}} \right) \quad (1)$$

where f_{gas} and f_{dust} are the fractions of Cr in gaseous and solid form respectively.⁵

The boxes with the heavy outline in Figure 6 show the abundances measured in the six intermediate redshift DLAs listed in Table 5. Two conclusions can be drawn from inspection of this Figure. First, the depletions of Cr, Fe and, when available, Ni are roughly comparable, as is the case in the local ISM (Savage & Sembach 1996).⁶ Second, the depletion levels are relatively modest, ranging from near-zero in Q0454+039 to a factor of ~ 4 in Q1351+318 ($\sim 25\%$ of Cr, Fe, and Ni in the gas). Such values are typical of DLAs in general (Pettini et al. 1997a), whereas in the disk of the Milky Way the same elements are depleted by more than one order of magnitude (see Figure 6 of Savage & Sembach 1996).

It is unclear what lies at the root of this difference. It is interesting that the ISM of the Small Magellanic Cloud also exhibits only mild depletions (Welty et al. 1997), but metallicity alone is unlikely to be the explanation, because there is no trend in our data for a dependence of [Zn/Cr] on [Zn/H] (for example Cr and Fe are depleted by only a factor of ~ 2 in Q0058+019, where [Zn/H] is approximately solar). In any case, it appears that in most DLAs the balance between the incorporation of refractory elements into, and their release from, dust grains is shifted relative to the physical conditions prevailing in cool disk clouds on the Milky Way, so that on average there are roughly equal proportions of these elements in gas and dust. Note that this is unlikely to be the result of dust-related selection effects analogous to those mentioned earlier (§4). The total column densities of metals in the DLAs studied here are too low to produce significant dust reddening, even if 100% of the elements which make up the grains were in solid form.

Finally on this topic, we point out that in two cases, Q0302–223 and Q0454+039, we can determine depletions separately for the two well resolved groups of components which make up the absorption lines (see Figures 4 and 5). The results are summarised in Table 6. Predictably, in Q0454+039 both components appear to be dust-free (since their sum is!). In Q0302–223, however, we see that the gas with the higher optical depth, at the adopted systemic redshift $z_{\text{abs}} = 1.00945$, has [Zn/Cr, Fe, Ni] $\simeq +0.6$, while in the component at $v = -36 \text{ km s}^{-1}$ the same ratio is only $\simeq +0.1$. Reduced depletions in interstellar clouds with high velocities are commonplace in

⁵Recently, Howk & Sembach (1999) have drawn attention to the fact that ionization effects may boost the $N(\text{Zn}^+)/N(\text{Cr}^+)$ ratio thereby mimicking dust depletion. However, this is unlikely to be the case for the DLAs considered here. Such effects would also increase the $N(\text{Ni}^+)/N(\text{Cr}^+)$ ratio by similar factors, contrary to our measurements. Based on the calculations by Howk & Sembach (1999), the observed [Ni/Cr] $\lesssim 0.0$ implies very low ionization parameters, as expected for clouds with $N(\text{H I}) \gtrsim 10^{20} \text{ cm}^{-2}$.

⁶The revision in the oscillator strengths of the Ni II lines mentioned in §4 has brought this element into better agreement with Fe and Cr, resolving an apparent puzzle which had been noted by Lu et al. (1996) and in Paper III.

the local ISM, where they have been known for nearly 50 years (Routly & Spitzer 1952) and are understood to arise from grain destruction in interstellar shocks.

6. ELEMENT RATIOS

Two of the elements covered by our observations, Si and Mn, exhibit metallicity dependent ratios (relative to Fe) in Galactic stars, presumably because their nucleosynthesis follows different channels from that of the Fe-peak group. Furthermore, in the local ISM both elements show a degree of dust depletion. When overall depletion levels are high, Mn and Si are normally less underabundant than Fe, Cr, and Ni. However, such differences become less pronounced as depletions are reduced (Figure 6 of Savage & Sembach 1996)—all elements tend to the same depletion as the overall depletion level approaches zero. If we restrict ourselves to cases where $[\text{Zn}/\text{Cr}] \lesssim 0.3$ (and therefore $f_{\text{dust}} \lesssim f_{\text{gas}}$ in eq. (1) so that dust correction factors are $\lesssim 2$), we may be justified in assuming that to a first approximation all refractory elements are depleted by the same factor.⁷ The boxes with the light outline in Figure 6 show element abundances corrected for the dust fractions implied by the observed $[\text{Zn}/\text{Cr}]$ ratios; in each case adopting the mean $[\text{Zn}/\text{Cr}, \text{Fe}, \text{Ni}]$ ratio would produce very similar results. We take these values to represent the total abundances (gas + dust) of the element concerned and, having made this correction, we can now proceed to compare the abundances of Si and Mn in DLAs of different metallicities with analogous measurements in Galactic stars.

The approach taken here is similar to, but more conservative than, the analysis by Vladilo (1998) who also used the ratio of Zn to Fe-peak elements to correct for dust depletion. The main difference is in the fact that Vladilo applied the correction to all DLAs for which relevant measurements were available, irrespectively of the degree of depletion, with the assumption that dust in DLAs has the same composition as in the Milky Way ISM. In our opinion we are on safer ground by limiting ourselves to cases where $f_{\text{dust}} \lesssim f_{\text{gas}}$ because our conclusions do not then depend sensitively on the unknown detailed make-up of interstellar dust at high redshift.

6.1. Silicon

The data for Si are displayed in Figure 7a, where the dots are the stellar measurements by Edvardsson et al. (1993) and Nissen & Schuster (1997). The general trend is for a mild increase in the relative abundance of Si at low metallicity; $[\text{Si}/\text{Fe}] \approx +0.2$ to $+0.3$ at $[\text{Fe}/\text{H}] \lesssim -1$. This is an example of the well known overabundance of the α -elements which is generally attributed

⁷In future it should be possible to test this assumption by measuring the abundance of S, an undepleted α -element. If the assumption is correct, we expect $[\text{S}/\text{Si}] = [\text{Zn}/\text{Cr}, \text{Fe}, \text{Ni}]$.

to the delayed production of additional Fe by Type Ia supernovae. In this picture, the overall metallicity (as measured by $[\text{Fe}/\text{H}]$) at which the ratio $[\alpha/\text{Fe}]$ begins to decline towards the solar value depends on the previous history of star formation. A galaxy which turns most of its gas into stars within ~ 1 Gyr (the generally assumed timescale for the explosion of Type Ia supernovae) would maintain an enhanced $[\alpha/\text{Fe}]$ ratio while $[\text{Fe}/\text{H}]$ grows to high values. Such a scenario may apply to the thick disk and the bulge of the Milky Way where recent observations seem to indicate a uniform enhancement of the α -elements at all metallicities (Fuhrmann 1998; Rich 1999, private communication). At the other extreme, in a galaxy where star formation proceeds slowly, or in bursts separated by quiescent periods lasting more than 1 Gyr, there would be time for $[\alpha/\text{Fe}]$ to decline to the solar value (or even lower) while $[\text{Fe}/\text{H}]$ remains low (Gilmore & Wyse 1991; Pagel & Tautvaisviene 1998).

Returning to Figure 7a, we now consider the evidence provided by DLAs. Triangles show our measurements from Table 5, corrected for dust as explained above and taking Zn as a proxy for Fe.⁸ We also searched the literature for other DLAs where the abundances of Zn, Cr, and Si have been measured and the ratio $[\text{Zn}/\text{Cr}]$ is within a factor of two of solar (therefore implying correspondingly small dust corrections). We found four such cases, all from the recent compilation by Prochaska & Wolfe (1999); they are shown in Figure 7a as large filled dots, again with the assumption that Cr and Si are depleted by similar amounts. The most straightforward conclusion from Figure 7a is that the $[\text{Si}/\text{Fe}]$ ratio in DLAs is not dissimilar from the values observed in Galactic stars. At least half of the DLA measurements fall well in line with the bulk of stellar data. There are also hints of differences, with two or three cases where $[\text{Si}/\text{Fe}]$ appears to be approximately solar at $[\text{Fe}/\text{H}] \lesssim -1$. While it is premature to make too much of these differences, it is probably fair to say that, unlike the situation for Galactic stars, one would not discern any trend in the $[\text{Si}/\text{Fe}]$ ratio with metallicity from the DLA results alone. Thus, the data available at present are certainly consistent with the view that damped Lyman α absorbers are drawn from a varied population of galaxies which may have processed their interstellar gas at different rates prior to the time when we observe them. On the other hand, blanket statements to the effect that the chemical histories of DLAs are different from that of the Milky Way (e.g. Vladilo 1998) do not seem to be fully justified on the basis of the data for Si in Figure 7a.

6.2. Manganese

A major new study of the abundance of Mn has recently been completed by Nissen et al. (2000) who measured $[\text{Mn}/\text{Fe}]$ in 119 Galactic F and G stars from the thin disk, the thick disk,

⁸This approach is preferable to using our Fe abundances directly, because the latter are based on very weak transitions with oscillator strengths which may be less secure than those of the Zn II doublet. The systematic underabundance by 0.2 dex of Fe relative to Cr in Figure 6 may well reflect the relative uncertainty in the f -values of the Cr II and Fe II lines.

and the halo, following the same method as Edvardsson et al. (1993) and making use of Hipparcos parallaxes where available. The analysis takes into account hyperfine structure splitting of the Mn I lines, which is one of the complications involved in bringing together different data sets from previous studies. The measurements by Nissen et al. are reproduced as small dots in Figure 7b. There is an obvious drop in $[\text{Mn}/\text{Fe}]$ with decreasing $[\text{Fe}/\text{H}]$; in the most metal-poor disk stars, at $[\text{Fe}/\text{H}] \simeq -1$, $[\text{Mn}/\text{Fe}] \simeq -0.4$. The physical processes responsible for the metallicity dependence of $[\text{Mn}/\text{Fe}]$ have not yet been confidently identified. Observers have remarked on the fact that the $[\text{Mn}/\text{Fe}]$ trend seems to mirror the overabundance of the α -elements but in the opposite sense (e.g. McWilliam 1997), leading to the conjecture that Type Ia supernovae may be an important source of Mn (Samland 1998; Nakamura et al. 1999). On the other hand, nucleosynthesis calculations can reproduce the shape of the trend in Figure 7b with a metallicity dependence yield of Mn in massive stars which in the calculations by Timmes, Woosley, & Weaver (1995) overwhelms the Type Ia contribution.

The filled triangles in Figure 7b show the values of $[\text{Mn}/\text{Fe}]$ determined for five of the DLAs considered in this paper, again taking Zn as the proxy for Fe for the reason explained above. From a literature search we found only one other data point which could be included in our analysis, in the $z_{\text{abs}} = 1.3726$ DLA towards Q0935+417 where $[\text{Zn}/\text{H}] = -0.80$, $[\text{Cr}/\text{H}] = -0.90$, and $[\text{Mn}/\text{H}] = -1.48$ (Meyer, Lanzetta, & Wolfe 1995; Pettini et al. 1997b). The comparison between stars and DLAs is complicated by the fact that there is still some uncertainty regarding the correct solar system value of the abundance of Mn. Anders & Grevesse (1989) quote $\log (\text{Mn}/\text{H}) = -6.61$ in the solar photosphere, but $\log (\text{Mn}/\text{H}) = -6.47$ from meteorites (the latter value is the one used in the present analysis). This discrepancy persists in the more recent reappraisal of ‘Standard Abundances’ by Grevesse, Noels, & Sauval (1996). The uncertainty in $(\text{Mn}/\text{H})_{\odot}$ does not affect the stellar data of Nissen et al. (2000) which are all derived from differential measurements, but it does mean that there is a 0.14 dex ambiguity in referring the DLA values to the stellar scale. Thus the triangles and filled large dot in Figure 7b may need to be raised by 0.14 dex should the meteoritic abundance determination turn out to be in error.

Even with this caveat, it does appear that Mn is underabundant in the galaxies producing damped Lyman α systems by factors similar to those measured in Galactic metal-poor stars. As in the case of Si, there are no obvious trends from the QSO absorption line data alone; $[\text{Mn}/\text{Fe}] \simeq -0.4 \pm 0.1$ is an adequate description of the whole DLA sample available at present. It is intriguing that the underabundance of Mn seems to persist to metallicities as high as solar, although admittedly such a statement is at present based on only one measurement. If further cases are found in future, the hypothesis that the underabundance of Mn is due to a metallicity-dependent yield in massive stars would clearly run into difficulties. On the other hand, finding that Mn is low ($[\text{Mn}/\text{Fe}] = -0.51$) in one DLA (in Q1354+258) which shows no enhancement of Si at low metallicity ($[\text{Fe}/\text{H}] = -1.61$ —see Figure 7), argues against the SN Type Ia interpretation, as also pointed out by Nissen et al. (2000). Possibly a third process, yet to be identified, is responsible for the metallicity dependence of the abundance of Mn.

7. CONCLUSIONS

We have measured element abundances in three galaxies which give rise to damped Lyman α systems at intermediate redshifts ($z \simeq 0.61 - 1.01$). The new data confirm the well established result that significantly smaller fractions of refractory elements are incorporated into dust grains in DLAs compared with interstellar clouds of similar column density in the disk of the Milky Way. Although the physical reasons underlying this effect are not fully understood, empirically it appears that the equilibrium between gas and dust in damped absorbers is shifted so that on average comparable proportions of the grain constituents are in gaseous and solid forms. We propose that in cases where dust depletions are less than a factor of about two, it is possible to account for the unobserved fractions of Si, Mn, Cr, Fe, and Ni by assuming that they are all depleted by approximately the same factor. This assumption then allows us to examine the dependence on metallicity of the intrinsic abundances of Si and Mn.

We find that the abundances of both elements are broadly in line with values measured in metal-poor stars of the Milky Way. In about half of the cases considered Si is mildly enhanced relative to Fe-peak elements at the typically lower-than-solar metallicities of the DLAs, but there are also counterexamples where $[\text{Si}/\text{Fe}]$ is more nearly solar even though $[\text{Fe}/\text{H}]$ is less than 1/10 solar. The underabundance of Mn at low metallicities is possibly even more pronounced than in Galactic stars, and no DLA has yet been found with a solar $[\text{Mn}/\text{Fe}]$. However, for neither element is there a clear abundance trend with metallicity; in our view this is an indication that galaxies picked by damped Lyman α absorption have experienced a variety of star formation histories prior to the time when we observe them. In this respect chemical abundances give a picture consistent with the results from imaging studies (including new observations reported here) which have shown that galaxies associated with DLAs exhibit a wide range of morphologies, luminosities, and surface brightnesses.

It is important to emphasize the preliminary nature of these conclusions which are based on the comparison of very few measurements in DLAs with a much larger body of stellar data. One of the lessons from stellar work is that there is considerable scatter, observational and intrinsic, in the relative abundances of different elements so that most trends only become apparent when a large set of observations has been assembled. As a field of study, abundance determinations in high redshift galaxies are some twenty years behind their counterparts in Galactic stars but they may well hold the key to clarifying some of the still unresolved issues on the origin of elements.

It is a pleasure to acknowledge the competent assistance with the observations by the staff of the Keck Observatory; special thanks are due to Tom Barlow for generously providing his echelle extraction software. We are very grateful to Poul Nissen and YuQin Chen for allowing us to use their stellar Mn abundances in advance of publication, and to Jim Lawler and Steve Federman for the early communication of their measurements of the f -values of Ni II transitions. This work has

benefited from several conversations with colleagues, particularly Ken'ichi Nomoto, Bernard Pagel, Jason X. Prochaska, and Sean Ryan. C. C. S. acknowledges support from the National Science Foundation through grant AST 94-57446 and from the David and Lucile Packard Foundation.

REFERENCES

- Anders, E., & Grevesse, N. 1989, *Geochim. Cosmochim. Acta*, 53, 197
- Carilli, C.L., Rupen, M.P., & Yanny, B. 1993, *ApJ*, 412, L59
- Edvardsson, B., Andersen, J., Gustafsson, B., Lambert, D.L., Nissen, P.E., & Tomkin, J. 1993, *A&A*, 275, 101
- Fedchak, J.A., & Lawler, J.E. 1999, *ApJ*, in press
- Folkes, S., et al. 1999, *MNRAS*, in press (astro-ph/9903456)
- Fruchter, A.S., & Hook, R.N. 1999, *PASP*, submitted (astro-ph/9808087)
- Fuhrmann, K. 1998, *A&A*, 338, 161
- Gilmore, G., & Wyse, R.F.G. 1991, *ApJ*, 367, L55
- Grevesse, N., Noels, A., & Sauval, A.J. 1996, in *Cosmic Abundances*, ed. S. Holt, & G. Sonneborn (San Francisco: ASP), 117
- Hawk, J.C., & Sembach, K.R. 1999, *ApJ*, submitted
- Kobayashi, C., Tsujimoto, T., Nomoto K., Hachisu, I., & Kato, M. 1998, *ApJ*, 503, 155
- Kobulnicky, H.A., & Zaritsky, D. 1999, *ApJ*, 511, 118
- Lanzetta, K.M., et al. 1997, *AJ*, 114, 1337
- Lanzetta, K.M., Wolfe, A.M., & Turnshek, D.A. 1995, *ApJ*, 440, 435
- Le Brun, V. Bergeron, J., Boissé, P., & Deharveng, J.M. 1997, *A&A*, 321, 733
- Lu, L., Sargent, W.L.W., Barlow, T.A., Churchill, C.W., & Vogt, S.S. 1996, *ApJS*, 107, 475
- McWilliam, A. 1997, *ARA&A*, 35, 503
- Meyer, D.M., & York, D.G. 1992, *ApJ*, 399, L121
- Meyer, D.M., Lanzetta, K.M., & Wolfe, A.M. 1995, *ApJ*, 451, L13
- Morton, D.C. 1991, *ApJS*, 77, 119
- Nakamura, T., Umeda, H., Nomoto, K., Thielemann, F.-K., & Burrows, A. 1999, *ApJ*, 517, 193
- Nissen, P.E., Chen, Y.Q., Schuster, W.J., & Zhao, G. 2000, *A&A*, submitted
- Nissen, P.E., & Schuster, W.J. 1997, *A&A*, 326, 751
- Pagel, B.E.J., & Tautvaisiene, G. 1998, *MNRAS*, 299, 535
- Pettini, M. & Bowen, D.V. 1997, *A&A*, 327, 22 (Paper II)
- Pettini, M., Ellison, S.L., Steidel, C.C., & Bowen, D.V. 1999, *ApJ*, 510, 576 (Paper III)
- Pettini, M., King, D.L., Smith, L.J., & Hunstead, R.W. 1997a, *ApJ*, 478, 536
- Pettini, M., Lipman, K., & Hunstead, R.W. 1995, *ApJ*, 451, 100
- Pettini, M., Smith, L.J., King, D.L., & Hunstead, R.W. 1997b, *ApJ*, 486, 665

- Prantzos, N., & Silk, J. 1998, *ApJ*, 507, 229
- Prochaska, J.X., & Wolfe, A.M. 1999, *ApJS*, in press (astro-ph/9810381)
- Rao, S.M., & Turnshek, D.A. 1998, *ApJ*, 500, L115
- Rosa, M.R., Kerber, F., & Keyes, C.D. 1998, FOS Instrument Science Report CAL/FOS-149
- Routly, P.M., & Spitzer, L. 1952, *ApJ*, 115, 227
- Ryan, S.G., Norris, J.E., & Beers, T.C. 1996, *ApJ*, 471, 254
- Samland, M. 1998, *ApJ*, 496, 155
- Savage, B.D., & Sembach, K.R. 1996, *ARA&A*, 34, 279
- Steidel, C.C., Bowen, D.V., Blades, J.C., & Dickinson, M. 1995, *ApJ*, 440, L45 (Paper I)
- Steidel, C.C., & Hamilton, D. 1993, *AJ*, 105, 2017
- Timmes, F.X., Woosley, S.E., & Weaver, T.A. 1995, *ApJS*, 98, 617
- Vladilo, G. 1998, *ApJ*, 493, 583
- Vogt, S.S. et al. 1994, *S.P.I.E.*, 2198, 362
- Welty, D.E., Lauroesch, J.T., Blades, J.C., Hobbs, L.M., & York, D.G. 1997, *ApJ*, 489, 672
- Wheeler, J.C., Sneden, C., & Truran, J.W. 1989, *ARA&A*, 27, 279
- Wiklind, T., & Combes, F. 1995, *A&A*, 299, 382
- Wolfe, A.M., Turnshek, D.A., Smith, H.E., & Cohen, R.D. 1986, *ApJS*, 61, 249
- Zsargó, J., & Federman, S.R. 1998, *ApJ*, 498, 256

Table 1. PROPERTIES OF THE CANDIDATE DLA ABSORBER IN Q0058+019^a

$\Delta\alpha(^{\prime\prime})$	$\Delta\delta(^{\prime\prime})$	$\theta(^{\prime\prime})$	$d^{\text{b,c}}$ (kpc)	R_s (mag)	M_B (mag) ^c	Comments
0.8	0.85	1.2	10.3	23.7	–19.1	Edge-on, late-type spiral

^aAssuming the galaxy to be at the DLA redshift $z_{\text{abs}} = 0.61251$

^bProjected separation from QSO sight-line

^c $H_0 = 50 \text{ km s}^{-1} \text{ Mpc}^{-1}$; $q_0 = 0.05$

TABLE 2
JOURNAL OF OBSERVATIONS

QSO	V (mag)	z_{em}	z_{abs}	Telescope	Instrument	Wavelength Range (Å)	Resolution (Å)	Integration Time (s)	S/N	$W_0(3\sigma)^a$ (mÅ)	$N(\text{H}^0)$ (10^{20} cm^{-2})
(1)	(2)	(3)	(4)	(5)	(6)	(7)	(8)	(9)	(10)	(11)	(12)
Q0058+019	16.6	1.961	0.61251	Keck I	HIRES	3210 – 4740	0.09	14,400	33	6	1.2 ± 0.5
Q0302–223	16.0	1.400	1.00945	Keck I	HIRES	3215 – 5325	0.09	10,800	55	3	2.3 ± 0.5
Q0454+039	16.5	1.350	0.85967	Keck I	HIRES	3340 – 4865	0.09	8,250	35	5	4.9 ± 0.7

^a 3σ detection limit for the rest frame equivalent width of an absorption line at z_{abs} with $\text{FWHM} = 10 \text{ km s}^{-1}$.

Table 3. COMPONENT STRUCTURE IN THE Fe II LINES

QSO	Component No.	z_{abs}	b (km s $^{-1}$)	$\log N(\text{Fe}^+) \text{ (cm}^{-2}\text{)}$
Q0058+019	1	0.612240	6.0	12.83
	2	0.612508	6.1	14.77
	3	0.612616	24.9	15.01
	4	0.612866	8.0	13.69
	5	0.612940	2.4	13.25
	6	0.613041	16.8	13.28
	7	0.613139	7.4	13.63
Q0302–223	1	1.009025	4.6	11.97
	2	1.009177	10.2	13.92
	3	1.009244	4.0	13.86
	4	1.009397	8.9	14.01
	5	1.009452	9.7	14.29
	6	1.009566	2.6	12.89
	7	1.009685	2.9	12.90
	8	1.010266	7.6	12.13
Q0454+039	1	0.859225	5.4	14.38
	2	0.859248	16.8	14.00
	3	0.859401	3.9	13.17
	4	0.859486	6.1	13.78
	5	0.859670	14.8	15.00
	6	0.859917	9.4	13.83
	7	0.860045	6.2	12.22

TABLE 4
ION COLUMN DENSITIES

QSO	z_{abs}	$\log N(\text{H}^0)$	$\log N(\text{Zn}^+)$	$\log N(\text{Si}^+)$	$\log N(\text{Mn}^+)$	$\log N(\text{Cr}^+)$	$\log N(\text{Fe}^+)$	$\log N(\text{Ni}^+)$
Q0058+019	0.61251	20.08 ± 0.15	12.81 C	...	13.12 A	13.57 B	15.24 A	...
Q0302-223	1.00945	20.36 ± 0.11	12.45 A	15.18 A	12.57 A	13.08 A	14.67 A	13.57 A
Q0454+039	0.85967	20.69 ± 0.06	12.33 B	15.45 B	12.91 A	13.49 A	15.17 A	...

NOTES.—Column densities are in units of cm^{-2} . A: Column density determined with an accuracy of better than 10%. B: Column density determined with an accuracy of between 10% and 20%. C: Column density determined with an accuracy of between 20% and 30%. D: Column density determined with an accuracy of between 30% and 50%.

TABLE 5
METAL ABUNDANCES RELATIVE TO SOLAR

QSO	z_{abs}	[Zn/H]	[Si/H]	[Mn/H]	[Cr/H]	[Fe/H]	[Ni/H]
Q0058+019	0.61251	$+0.08 \pm 0.21$...	-0.49 ± 0.16	-0.19 ± 0.18	-0.35 ± 0.16	...
Q0302-223	1.00945	-0.56 ± 0.12	-0.73 ± 0.12	-1.32 ± 0.12	-0.96 ± 0.12	-1.20 ± 0.12	-1.04 ± 0.12
Q0454+039	0.85967	-1.01 ± 0.12	-0.79 ± 0.12	-1.31 ± 0.08	-0.88 ± 0.08	-1.03 ± 0.08	...
Q1247+267	1.22319	-1.05 ± 0.25	-1.14 ± 0.15	-1.61 ± 0.10	-1.25 ± 0.15	-1.42 ± 0.10	≤ -1.51
Q1351+318	1.14913	-0.36 ± 0.17	-0.55 ± 0.17	-1.16 ± 0.13	-0.93 ± 0.17	-1.00 ± 0.12	≤ -1.02
Q1354+258	1.42004	-1.61 ± 0.16	-1.73 ± 0.15	-2.32 ± 0.09	-1.81 ± 0.09	-2.03 ± 0.08	-2.28 ± 0.09

NOTES.—[X/H] = $\log [N(X)/N(H)]_{\text{DLA}} - \log [N(X)/N(H)]_{\odot}$. The compilation of solar (meteoritic) abundances by Anders & Grevesse (1989) was adopted throughout.

TABLE 6
METAL ABUNDANCES IN SEPARATE ABSORPTION COMPONENTS

QSO	z_{abs}	v (km s $^{-1}$)	[Zn/Si]	[Zn/Mn]	[Zn/Cr]	[Zn/Fe]	[Zn/Ni]
Q0302–223	1.00945	0	0.25	0.84	0.52	0.75	0.58
		–36	–0.12	0.43	0.01	0.25	0.12
Q0454+039	0.85967	0	–0.15	0.37	–0.07	0.09	...
		–70	≤ -0.01	≤ 0.51	≤ 0.09	≤ 0.19	...

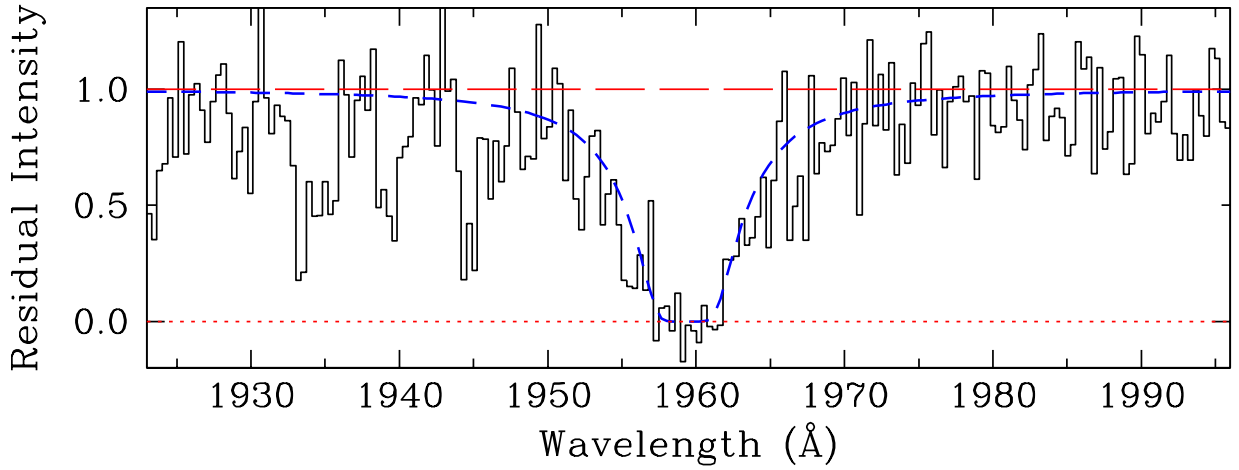


Fig. 1.— Portion of the G270H FOS spectrum of Q0058+019 (PHL 938) encompassing the damped Lyman α line in the $z_{\text{abs}} = 0.61251$ system. The resolution is $\sim 2 \text{ \AA}$ FWHM and $S/N \approx 7$; the exposure time was 1590 s. The short-dash line shows the theoretical damping profile for a column density $N(\text{H}^0) = 1.2 \times 10^{20} \text{ cm}^{-2}$.

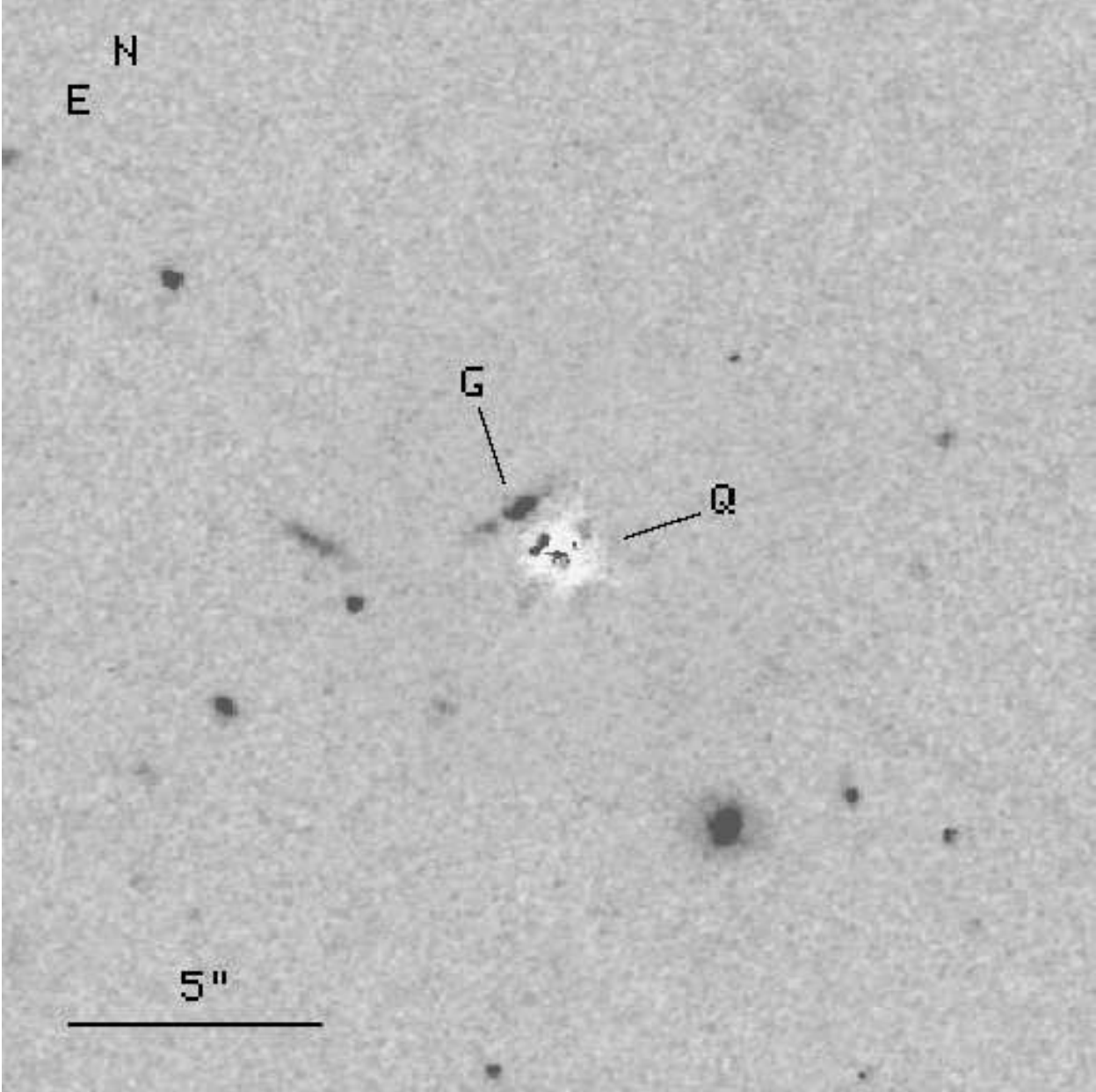


Fig. 2.— WFPC2 F702W exposure of the field of Q0058+019 (PHL 938). North is at the top and East is to the left. A model point spread function has been subtracted from the QSO image as described in the text, revealing the presence of a galaxy approximately 1.2 arcseconds to the NE of the QSO position. Given its proximity, this is likely to be the damped Lyman α absorber at $z = 0.61251$. Residual excess absorption of a diffraction spike cuts across the galaxy image. When this processing artifact is taken into account, the candidate absorber appears to be a low luminosity ($L \simeq 1/6L^*$) late-type galaxy seen at high inclination, $i \approx 65^\circ$, at a projected separation of $10 h_{50}^{-1}$ kpc from the QSO sight-line. Other relevant measurement are collected in Table 2.

Q0058+019 $z_{\text{abs}}=0.61251$

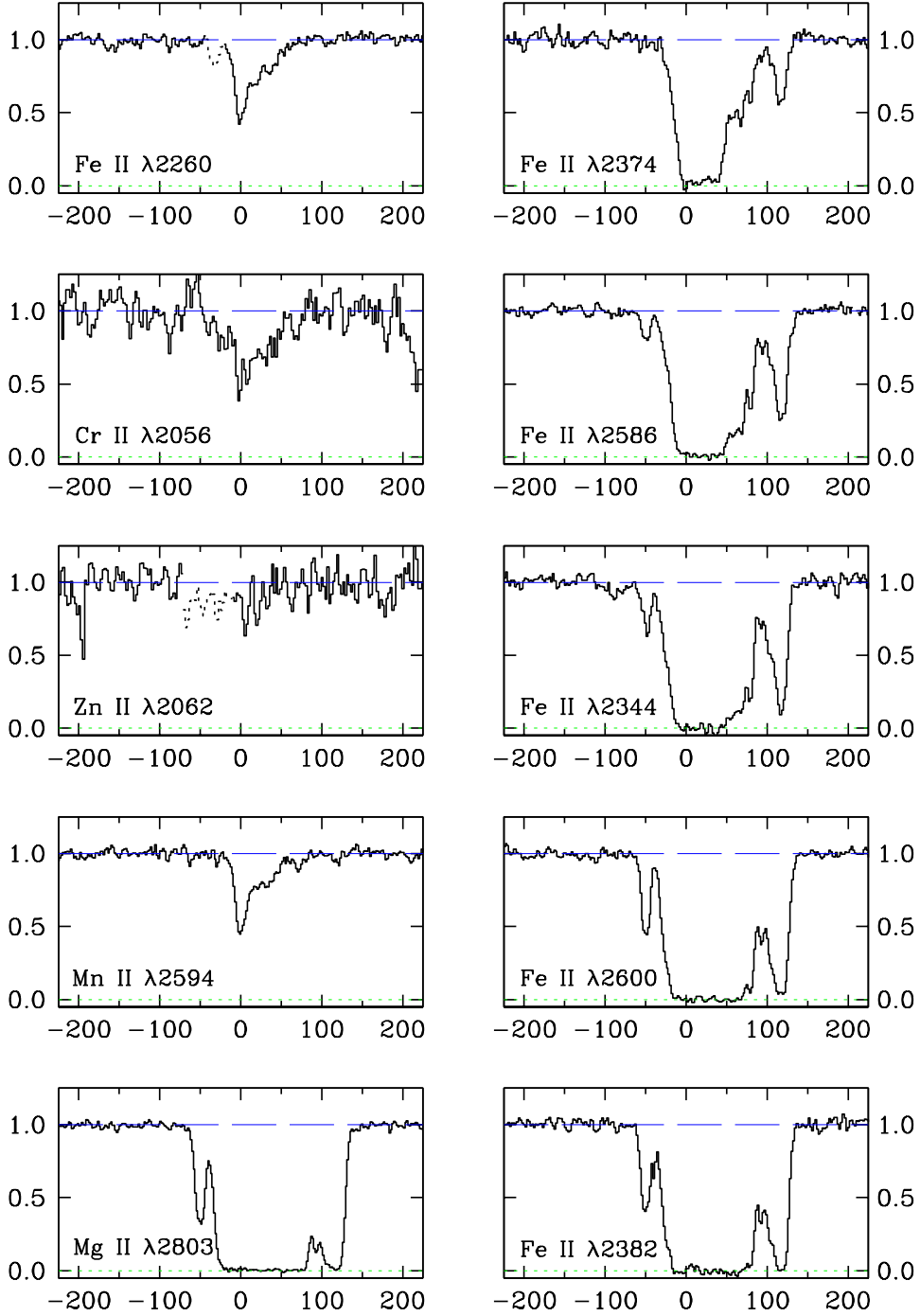


Fig. 3.— Profiles of selected absorption lines in the $z_{\text{abs}} = 0.61251$ DLA in Q0058+019. The y -axis is residual intensity; the x -axis is velocity in km s^{-1} relative to z_{abs} , defined from the centroid of the component with the highest optical depth.

Q0302–223 $z_{\text{abs}} = 1.00945$

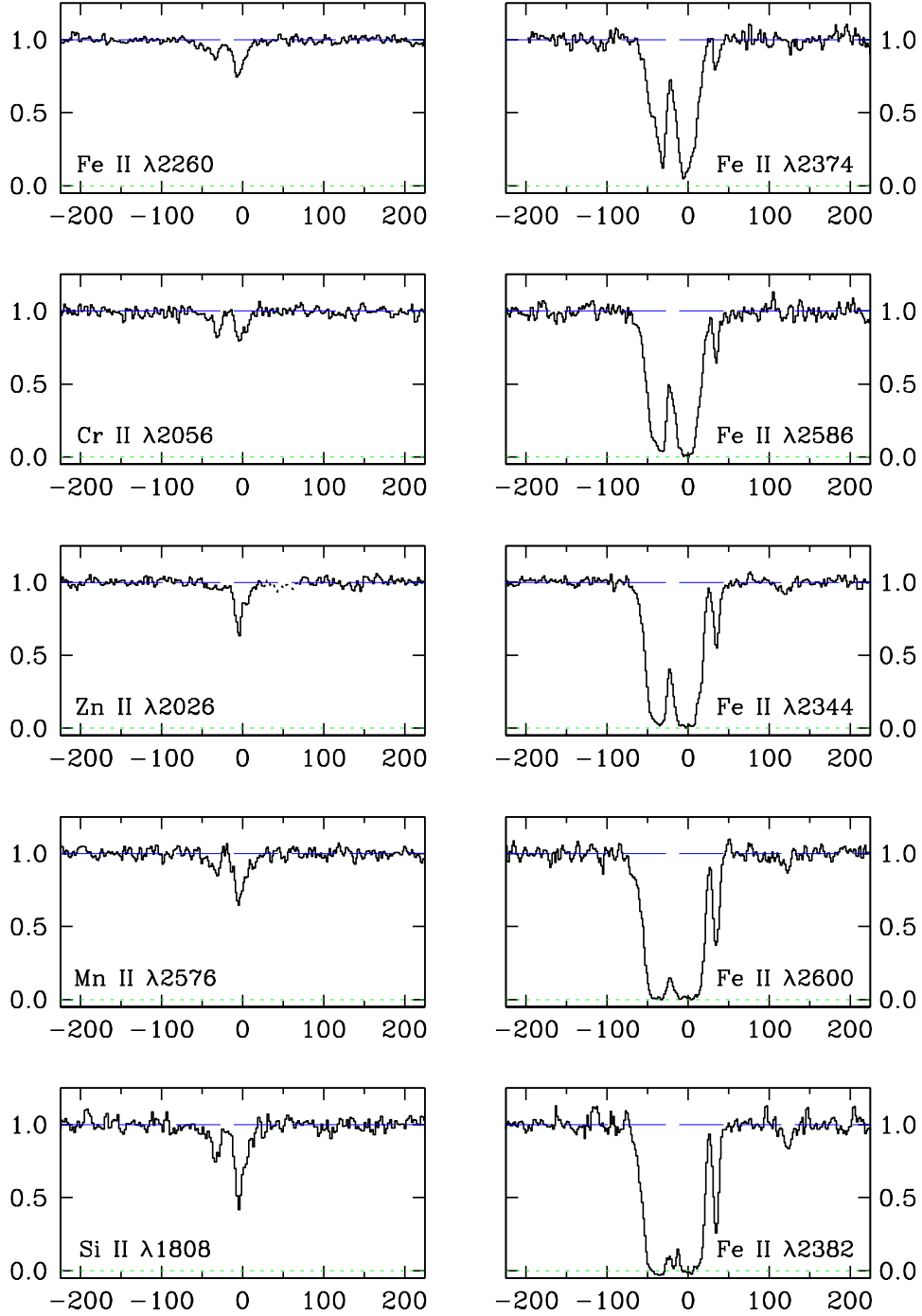


Fig. 4.— Profiles of selected absorption lines in the $z_{\text{abs}} = 1.00945$ DLA in Q0302–223. The y -axis is residual intensity; the x -axis is velocity in km s^{-1} relative to z_{abs} , defined from the centroid of the component with the highest optical depth.

Q0454+039 $z_{\text{abs}}=0.85967$

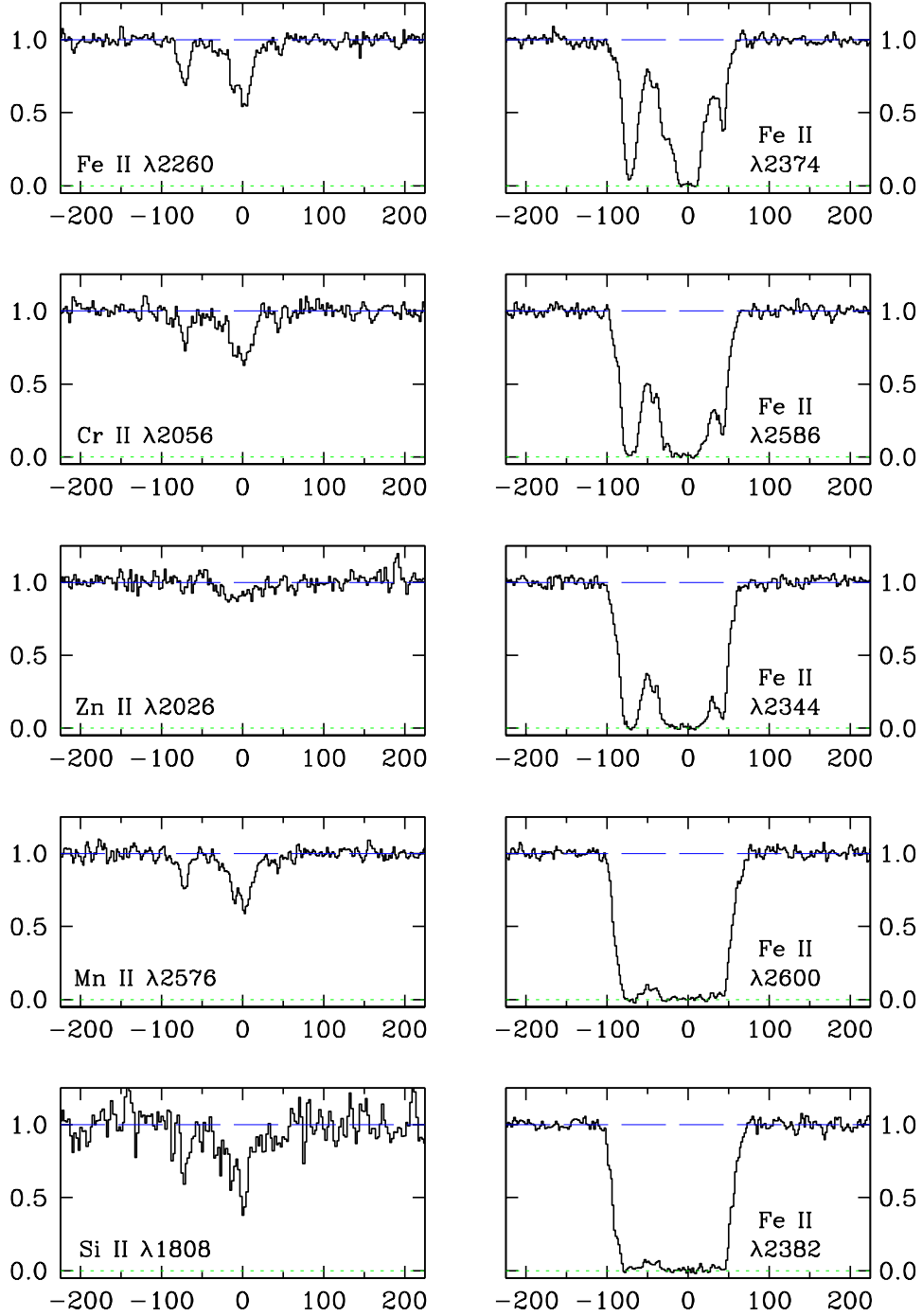


Fig. 5.— Profiles of selected absorption lines in the $z_{\text{abs}} = 0.85967$ DLA in Q0454+039. The y -axis is residual intensity; the x -axis is velocity in km s^{-1} relative to z_{abs} , defined from the centroid of the component with the highest optical depth.

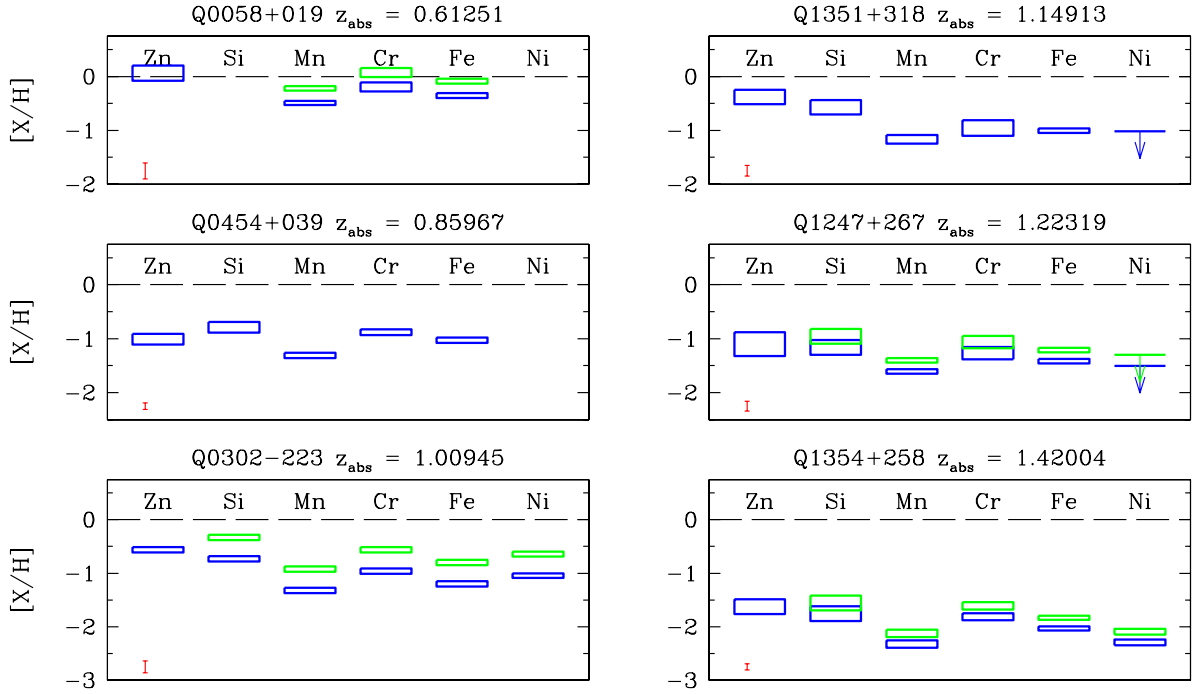


Fig. 6.— Element abundances in intermediate redshift DLAs from this paper and from Paper III are plotted on a logarithmic scale relative to solar values. The height of each box represents the uncertainty in the column density of that element; the vertical bars near the bottom left hand corners of the panels indicate the errors in the column densities of neutral hydrogen. Boxes with heavy outline (blue in the colored version of this figure) show the measured values; boxes with a light (green) outline are the values corrected for dust depletion. No dust correction is required for Q0454+039 where $[\text{Zn}/\text{Cr}] \simeq 0$ within the errors. We have not corrected the measurements for Q1351+318 because here depletions are greater than a factor of two and the assumption that all refractory elements are depleted by the same amount may break down.

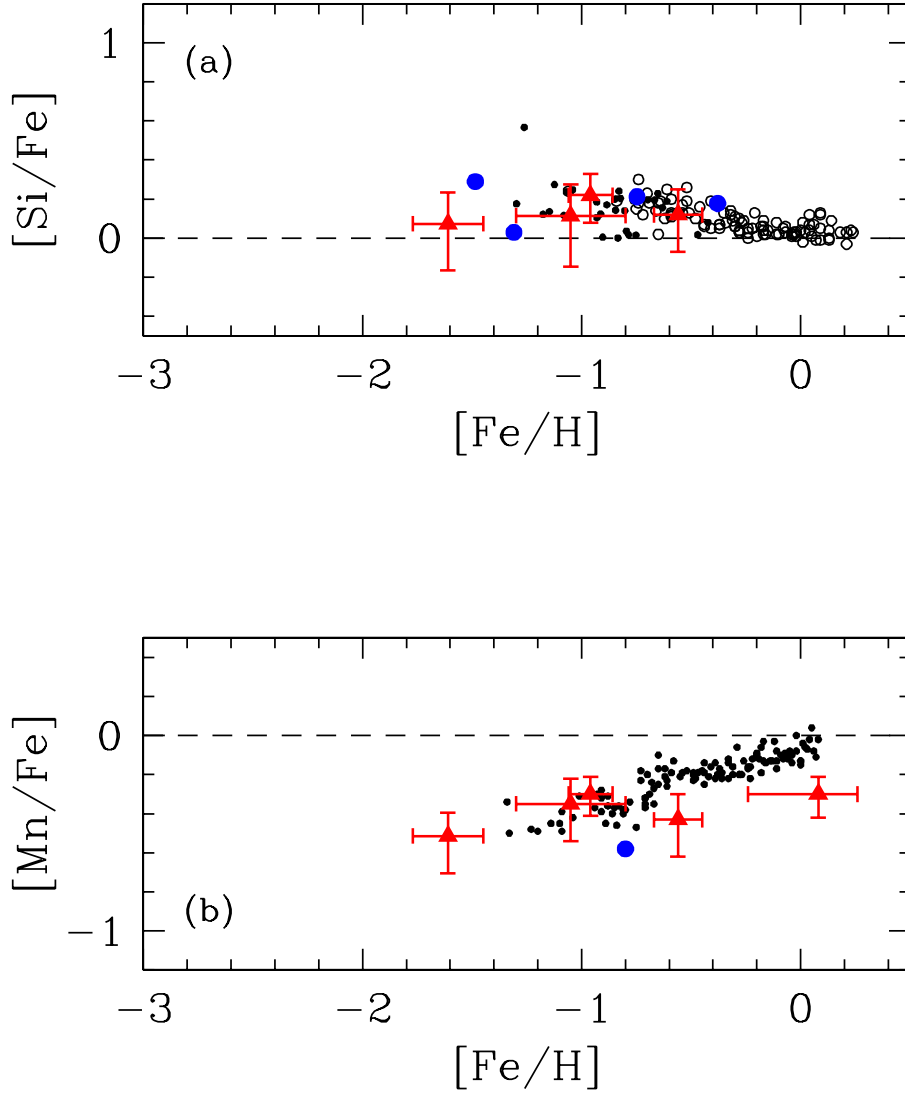


Fig. 7.— Metallicity dependence of the abundances of Si and Mn. Small dots are values in Galactic stars. For Si we have reproduced the stellar data from the compilations by Edvardsson et al. (1993; open dots) and Nissen & Schuster (1997; filled dots); to avoid overcrowding in the figure we have only plotted one out of every two measurements by Edvardsson et al. For Mn we show the results of the recent survey by Nissen et al. (2000). The other symbols refer to damped Lyman α systems observed by us (triangles), or by others (large dots); Zn has been taken as a proxy for Fe. The DLAs shown are cases where the corrections for the fractions of Si and Mn locked up in grains are less than a factor of two.